Use of Detrital-zircon U–Pb age-distribution Comparison to Infer Source Location

Jialin Wang
Peking University
Chaodong Wu (cdwu@pku.edu.cn)
Peking University
Yue Jiao
Peking University
Bo Yuan
Xinjiang Oilfield Company

Research Article

Keywords: Detrital-zircon U–Pb dating, Source-to-sink, Syndepositional volcanic activity, Southern Junggar Basin, the Bogda Mountains

Posted Date: April 14th, 2021

DOI: https://doi.org/10.21203/rs.3.rs-418142/v1

Abstract

Provenance analysis for volcanism without field evidence remains a major challenge. Detrital zircon grains from 13 samples of the Middle–Upper Triassic Xiaoquangou Group in the Southern Junggar Basin (SJB) were analyzed using U–Pb geochronology to constrain the location and characteristics of Triassic volcanism in the area as well as to understand its tectonic implications. A comparison of the distribution of detrital zircon U–Pb ages reveals Triassic zircon ages predominate in northern Bogda Mountains, with subordinate contributions also in southern Bogda Mountains, and no or minimal input in North Tianshan piedmont. The geochronology data combined with the euhedral and angular zircon grains suggest that the Triassic zircons probably originate from Bogda Mountains. A comparative provenance analysis reveals varied sources for Xiaoquangou Group in the SJB, with sediments of the Bogda Mountains area derived mainly from North Tianshan, Central Tianshan, and Bogda Mountains. The supply of sediments from Bogda Mountains started in the Late Triassic, and is indicative of the initial uplift of Bogda Mountains. This study proves the effectiveness of the comparison of detrital zircon U–Pb age distributions for inferring source characteristics and is applicable in similar situations, particularly when the source area is poorly preserved.

1. Introduction

Detrital zircon U–Pb geochronology is widely exploited for source-to-sink analysis (e.g. Cawood and Nemchin 2000; Hoskin and Ireland 2000; Belousova et al. 2002; Anderson 2005; Cawood et al. 2012; Nie et al. 2012; Liu et al. 2013, 2017, 2018; Yang et al. 2013; Gehrels 2014; Tang et al. 2014; Bhattacharya et al. 2016; Romans et al. 2016; Wu et al. 2017; Nguyen et al. 2018; Olierook et al. 2019; Wang et al. 2018b, 2019b). The rationale for the method is the similarity of zircon U–Pb age distribution patterns from the source and sink areas (Fig. 1; Nie et al. 2012; Romans et al. 2016). However, limitations emerge when direct evidence of related detrital zircon U–Pb ages is missing for the potential source areas or when the source areas are poorly preserved (Fig. 1; Romans et al. 2016 and references therein). As shown in Fig. 1, the detrital zircon U–Pb age pattern reveals an age group “D”, with no related magmatic rocks in potential source areas. This situation is common for deep-time source-to-sink analysis due to intense denudation in source areas and poor exposure of stratigraphic record (Sømme, and Jackson 2013; Sømme et al. 2013; Hampson et al. 2014; Michael et al. 2014; Romans et al. 2016). Therefore, confirmation of the provenance in such a situation remains challenging, with no satisfactory method to solve the problem.

In recent years, many zircons of Middle–Late Triassic age were found in sediments from the Xiaoquangou Group of Bogda Mountains (Wang et al. 2018b, 2019b), but no or limited Triassic volcanism reports exist for Junggar Basin and adjacent areas. The Middle–Late Triassic zircons showed similar ages to the Xiaoquangou Group, indicating syn-depositional magmatic activity. These zircons initially appeared in the Middle Triassic Kelamayi Formation, and mostly appeared in the Upper Triassic Haojiagou Formation. Moreover, the detrital zircon U–Pb age distribution patterns of the Upper Triassic Haojiagou Formation changes abruptly compared to the underlying strata, with a multimodal age spectrum (Wang et al. 2018b, 2019b). These phenomena highlight the importance of the Triassic zircons

provenance for understanding the tectonic evolution of the region (Ji et al. 2018; Wang et al. 2018b, 2019b). The presently exposed geology of potential source regions does not include Triassic age igneous rocks and therefore there is no way to correlate the existence of such grains in sandstones with a source area. These Triassic zircons, nevertheless, has been interpreted as derivation from the Jiumusaer area of the Bogda Mountains (BGMRXUAR, 1993), Central Tianshan (Yin et al. 2018), and Harlik Mountains (Ji et al. 2018).

In this contribution, we assess the provenance of the Middle–Upper Triassic Xiaoquangou Group in southern Junggar Basin (SJB) through a comparison of the detrital zircon U–Pb age distributions of thirteen samples which collected from different sink areas. These areas included the Sikeshu, Jiangongmeikuang, Aiweiergou, Haojiagou, Jingjingzigou, Haxionggou, Baiyanghe, Xidalongkou, Dongdalongkou, Taodonggou, Dabancheng and Yuergou sections, and Well C regions (12 sections and 1 well in total). The emphasis of this study is to explore an approach to infer the source location in the absence of direct field evidence for related detrital-zircon U–Pb ages of the potential source area. It also utilizes other information (e.g. trace elements contents) from the detrital zircons to further characterize the source features.

2. Geological Setting

The Junggar Basin is a triangular-shaped sedimentary basin surrounded by the West Junggar Mountains in the northwest, the East Junggar Mountains in the northeast, and the Chinese Tianshan and Bogda Mountains in the south (Fig. 2; Carroll et al. 2012). The basin and adjacent areas are part of the Central Asian Orogenic Belt (CAOB) formed through the accretion of island arcs, ophiolites, and micro-continental fragments (Şengör et al. 1993; Windley et al. 2007; Xiao et al. 2008, 2013). In the Palaeozoic, the Junggar Basin, together with the surrounding Bogda rift, West Junggar systems, East Junggar Mountains, Turpan–Hami Basin, and North Tianshan Ocean belonged to the southern part of Paleo–Asian Ocean, composed of the Ob–Zaisan, Junggar–Balkhash, and Turkestan Oceans from north to south (Filippova et al. 2001; Korobkin and Buslov 2011; Li et al. 2016). The SJB (including the present North Tianshan and Bogda Mountains areas), represent the southern part of the Junggar–Balkhash Ocean in the CAOB, surrounded by the North Tianshan Arc, Central Tianshan Block, East Junggar Arc (Harlik–Dananhu Arc), and West Junggar systems (Han et al. 2010; Han and Zhao 2018).

The SJB was characterized by rifting in the Permian (Carroll et al. 1995; Greene et al. 2001, 2005; Wartes et al. 2002; Fang et al. 2006; Yang et al. 2007, 2010; Wang et al. 2016, 2018b, 2019a, 2019b) and followed by drifting in the Triassic (Yang et al. 2007, 2010; Wang et al. 2016, 2018b, 2019a, 2019b). Sedimentological analysis shows that the sedimentary environments of SJB in the Permian comprise marine and continental facies with frequent lateral facies and thickness changes (Yang et al. 2007, 2010; Obrist-Farner and Yang 2015, 2017; Wang et al. 2016, 2019a, 2019b). Moreover, various areas display unique sedimentary characteristics, suggesting numerous sub-basins composed of a series of half-grabens and/or grabens (Obrist-Farner and Yang 2017; Wang et al. 2019b). In the Triassic, the strata of the SJB principally included fluvial and lacustrine facies sweeping into an intracontinental basin (Fig. 3;

Wang et al. 2016). The potential source areas are inferred to be in the south including the North Tianshan (NTS), Central Tianshan (CTS), South Tianshan (STS), and Bogda Mountains (Li et al. 2012; Tang et al. 2014; Wang et al. 2018b, 2019a, 2019b) based on predominantly northeast or north trending paleocurrents (Zhu et al. 2017; Wang et al. 2019b and references therein).

The NTS is composed of arc-related igneous and volcaniclastic rocks of Devonian to Carboniferous age, which have been interpreted as products of the southward subduction of the NTS oceanic crust during the late Paleozoic (Gao et al. 1998; Han et al. 2010; Xiao et al. 2013; Wang et al. 2017, 2018a). The CTS was a continental block with Precambrian basement, and is considered as a product of the northern and southern magmatic belts (Gao et al. 1998). The tectonostratigraphic units of CTS comprise Proterozoic basement and early Paleozoic arc-type rocks intruded by late Paleozoic granitoids (Han et al. 2010, 2011). The Bogda Mountains, like the northern part of the NTS (Fig. 1*c*) contain mainly Devonian to Quaternary sedimentary and igneous rocks (Allen et al. 1995; Gao et al. 1998). Among these, Carboniferous bimodal volcanic rocks are widely distributed (Gu et al. 2000, 2001), while sedimentary rocks primarily include siliciclastics, carbonates, and volcanic breccia, characterized by the absence of or minor quantities of quartzose sandstone or ophiolite (BGMRXUAR 1993).

3. Sampling And Analytical Methods

Medium- to coarse-grained sandstones were collected from eight sections of the Middle–Upper Triassic Xiaoquangou Group in SJB for detrital zircon U–Pb analysis (Fig. 2*b*). The samples including 12SKS-07, 17JGMK-06, XJ12-06, 17HJG-01, 15HXG-95, 17JJZG-10, 17BYH-61, 16DLK-49, 17DDLK-09, 16TDG-06, 16DBC-04, HX-01, and 15C-33 are from the Sikeshu section, Jiangongmeikuang section, Aiweiergou section, Haojiagou section, Haxionggou section, Jingjingzigou section, Baiyanghe section, Xidalongkou section, Dongdalongkou section, Taodonggou section, Dabancheng section, Yuergou section, and Well C, respectively. The detrital zircon U–Pb age data for samples 12SKS-07 (T_3xq), XJ12-06 ($T_{2+3}xq$), 15C-33 (T_3hj), 16DLK-49 (T_3hj), and HX-01 ($T_{2+3}xq$) are from Zhu et al. (2017), Liu et al. (2013), Wang et al. (2018b), Wang et al. (2019b), and Liu et al. (2017), respectively. The data for samples 17JGMK-06 ($T_{2+3}xq$), 17HJG-01 (T_3hj), 15HXG-95 ($T_{2+3}xq$), 17JJZG-10 ($T_{2+3}xq$), 17BYH-61 (T_2k), 17DDLK-09 (T_2k), 16TDG-06 (T_3xq), and 16DBC-04 (T_3xq) were generated in this study.

Detrital zircon grains were separated using standard heavy-liquid and magnetic techniques, followed by random purification of 250 zircon grains under a binocular microscope. The grains then underwent cathodoluminescence (CL) imaging and U–Pb isotope analyses by LA–ICP–MS at the Key Laboratory of Orogenic Belts and Crustal Evolution, Peking University and Rockman technology Co., Ltd microanalysis lab, Beijing, with detailed procedures following Yuan et al. (2004) and Thompson et al. (2018). The isotope ratios and the elements concentrations of the zircon grains were calculated using the GLITTER 4.0 program (Jackson et al. 2004). Correction for common lead used the method of Andersen (2002) and the ages were computed using ISOPLOT 3 (Ludwig 2003).

4. Results

4.1 Zircon U–Pb ages

Detrital zircon U–Pb ages for the thirteen samples (12SKS-07, 17JGMK-06, XJ12-06, 17HJG-01, 15HXG-95, 17JJZG-10, 17BYH-61, 16DLK-49, 17DDLK-09, 16TDG-06, 16DBC-04, HX-01, and 15C-33) from various sections are given in Supplemental Table 1. The relative ages from the U–Pb concordia and the probability density of zircon U–Pb age distributions are plotted in Figs. 4 and 5, respectively. Most of the zircon grains exhibit oscillatory zoning, low luminescence, and high Th/U ratios (>0.1), diagnostic of a magmatic origin (Supplemental Table 1; Corfu et al. 2003). The zircon showing >10% discordance is excluded from the interpretation (Supplemental Table 1).

Detrital zircon ages for the samples are categorized into six populations including the Precambrian (>542 Ma), Cambrian–Devonian (541–361 Ma), Mississippian (360–320 Ma), Pennsylvanian (320–300 Ma), Permian (300–250 Ma), and Triassic (250–200 Ma; Fig. 5; Supplemental Table 1). The sediments of the Middle–Upper Xiaoquangou Group from the Sikeshu (sample 12SKS-07) and Jiangongmeikuang (sample 17JGMK-06) sections predominantly contain Carboniferous zircons, mostly in the Pennsylvanian (320–300 Ma) age group (Fig. 5). The sediments from the Aiweiergou (sample XJ12-06), Taodonggou (sample 16TDG-06) and Dongdalongkou (sample 17DDLK-09) sections, on the contrary, show higher proportions of Mississippian zircons with ages from 360–320 Ma (Fig. 5). The sediments from the Haxionggou section (sample 15HXG-95), Jingjingzigou section (sample 17JJZG-10), and Baiyanghe section (sample 17BYH-61) show two major peaks with age groups of both Pennsylvanian and Mississippian.

The detrital zircon U–Pb age patterns for the Haojiagou section, Xidalongkou section, Dabancheng section, Yuergou section and Well C are similar, with the principal age peaks and the relative proportions of age groups comparable for various locations (Fig. 5). The samples from the Well C (sample 15C-33), Haojiagou section (sample 17HJG-01) and Xidalongkou section (sample 16DLK-49) show multiple age peaks characteristic of all age groups (>542–200 Ma; Fig. 5). The sediments from both sections yield age patterns dominated by Triassic populations, with subordinate populations of Mississippian, Pennsylvanian, and Permian ages. The sediments of the Dabancheng and Yuergou sections display relatively lower proportions of Triassic populations, with sample 16DBC-04 from the Dabancheng section yielding age patterns dominated by the Pennsylvanian, accompanied by subordinate Cambrian–Devonian, Mississippian, and Triassic populations. The age groups for sample HX-01 (the Yuergou section) are dominated by the Mississippian, with minor Cambrian–Devonian, Pennsylvanian, Permian, and Triassic constituents (Fig. 5).

4.2 Zircon trace elements

Results from geochemical analysis of the detrital zircons are listed in Supplemental Table 2. The zircons show a wide range of rare earth elements (REEs) concentrations (218–10178 ppm, mostly 400–900

ppm), with the average concentrations significantly above that for chondrite (2.65 ppm; Sun and McDonough, 1989). Most of the zircons, irrespective of the age groups, are depleted in light REEs and enriched in heavy REEs as displayed in the chondrite plots (Fig. 6; Sun and McDonough, 1989). Majority of the analyzed zircons exhibit negative Eu and positive Ce anomalies (Fig. 6; Supplemental Table 2; Eu/Eu^{*} = 0.01–0.72; Ce/Ce^{*} = 1.1–357.8), which also diagnostic of a magmatic origin (Hoskin and Ireland 2000; Belousova et al. 2002; Corfu et al. 2003; Wang and Li 2017). The Triassic zircons (Fig. 6*a*) show similar REEs concentrations and chondrite–normalized patterns to the Cambrian–Permian zircons (Fig. 6*b–f*; Supplemental Table 2).

5. Discussion

5.1 Provenance of the Triassic zircons: location and composition

The detrital zircon U–Pb ages for the eight samples from the Middle–Upper Triassic Xiaoquangou Group in SJB are categorized into six populations displayed in Fig. 5. Previous studies on paleocurrents show that the potential source areas lie south of the Tianshan Mountains (Li et al. 2012; Yang et al. 2013; Tang et al. 2014; Zhu et al. 2017; Liu et al. 2013, 2017; Wang et al. 2018b, 2019b). Therefore, a comparison of the detrital zircon U–Pb age distribution to the reported crystallization ages of intermediate–acidic igneous rocks from the NTS, CTS, Bogda Mountains, and STS–Tarim, enables determination of the provenance of Cambrian to Permian detrital zircons (Fig. 5; Wang et al. 2018b, 2019b). However, constraining the provenance of Triassic zircons is difficult because reports suggest limited or no Triassic magmatism in the Junggar Basin and adjacent areas. Greene et al. (2005) reported a granitoid pluton zircon U–Pb age of 229 ± 11 Ma for the Barkol Tagh (Eastern Tianshan). Yin et al. (2018) reported a biotite $^{40}Ar–^{39}Ar$ age of 239.5 ± 1.3 Ma for the CTS, while zircon U–Pb age yielded an age of 281.9 ± 1.2 Ma for the same sample. The BGMRXUAR (1993) reported thin amygdaloidal andesites interlayered with the Middle Triassic Kelamayi Formation in the Jimusaer area of Bogda Mountains, without providing precise ages. That is, direct field evidence of Triassic magmatic activity in the area is inexistent.

Constraining the provenance of Triassic zircons was in addition to dating the main reason for collecting the samples from west to east in different sections of SJB (Fig. 2). The detrital zircon U–Pb dating results reveal dominance of Triassic zircons in the Haojiagou and Xidalongkou sections (northern Bogda Mountains), with subordinate populations in the Well C, and Dabancheng and Yuergou sections (southern Bogda Mountains), and no or minor amounts in other regions like the NTS and CTS areas (e.g. the Sikeshu, Jiangongmeikuang, and Aiweiergou sections; Fig. 5). The proportions of the Triassic zircons decrease steadily from the Well C, and Haojiagou and Xidalongkou sections to the Dabancheng and Yuergou sections, and further in the Aiweiergou and Jiangongmeikuang sections (Figs. 2 and 5).The Triassic detrital zircons occur mainly in the Middle–Upper Triassic Xiaoquangou Group of west Bogda Mountains, with absence in the NTS and CTS areas, suggesting the Triassic zircons probably come from

the Bogda Mountains, restricted to the Urumqi–Jimusaer region, and probably in the Haojiagou–Well C–Xidalongkou areas.

Moreover, some other evidences support that the Triassic zircons are probably source from the Bogda Mountains. (1) Paleocurrent observations show complicated drainage system with both northward- and southward-directed paleocurrents (Fig. 8). The paleocurrents are principally perpendicular to the present day Bogda Mountains in the western Bogda Mountains, while in the eastern Bogda Mountains the paleocurrents mainly northward-directed (Fig. 8). This proved that the western Bogda Mountains probably have uplifted and began to provide sources. Instead, the eastern Bogda Mountains (e.g., Zaobishan region) remain accept as a sink region with the sources from NTS and CTS. (2) The shapes of lithic fragments and Triassic zircon grains are angular to sub-angular (Fig. 7; Wang et al., 2018b), maybe indicate a proximal source area. The sedimentary lithic fragments occur in the Middle–Upper Triassic samples and increase upward with decrease in feldspar grains (Wang et al., 2018b), suggest less unroofing of granitoids and more unroofing of clastic rocks. These phenomena indicate that the Middle–Late Triassic provenance are probably come from the nearby Bogda Mountains which provide syndepositional and recycled sediments.

In addition, some problems worth discussing. (1) About the location of source area: We attribute the Triassic zircons to the Bogda Mountains which are likely interlayered in the Middle–Upper Triassic Xiaoquangou Group as suggested by BGMRXUAR (1993). Greene et al. (2005) reported the Triassic granitoid plutons in the Barkol Tagh region (Eastern Tianshan), further confirmed the Triassic magmatic activity exist in the Tianshan region. Theoretically, both locations could be the provenance of Triassic zircons, but petrological characters do not support Barkol Tagh region because it is too far to provide sources to the western Bogda Mountains (Fig. 3). Instead, the Balikun area maybe accepted deposits from the Barkol Tagh as shown by the paleogeographic map (Fig. 3). (2) About the composition of provenance: The trace element compositions of the detrital zircons are sensitive to source rock type (Hoskin and Ireland, 2000; Belousova et al. 2002; Corfu et al. 2003; Yang et al. 2012; Wang and Li, 2017). The variations of representative elements and ratios of REEs for the zircons indicate that the Triassic zircons originated from intermediate–acidic igneous rocks, with probable dominance of intermediate igneous rocks (Fig. 9). This inference is further supported by the REEs abundance and chondrite–normalized REE patterns (Fig. 6). The Triassic zircons show close REEs concentrations and chondrite–normalized REE patterns to the Cambrian–Permian zircons, suggesting they were derived from similar source rock types (Fig. 6; Hoskin and Ireland 2000; Belousova et al. 2002). Previous researches attest that the Cambrian–Pennsylvanian and Permian zircons were likely sourced from the intermediate–acidic igneous rocks of the NTS and CTS (Wang et al. 2018b, 2019a, 2019b). Collectively, the Triassic zircons are of magmatic origin and credibly originate from the intermediate–acidic igneous rocks. (3) About the explanation of previous work: Tang et al. (2014) published detrital zircon spectrum for sample TS12-99, which mark as Lower Triassic strata in the map but introduce as Middle–Upper Triassic Xiaoquangou Group in the text. Actually, it should be Lower Triassic strata after communicated with the author. Fang et al. (2015) think their published sample Hao-01 is collected from the Middle–Upper Triassic Xiaoquangou Group, but the latitude and longitude (N43°39.128', E87°13.229') of this sample shows that it is collected

from the Lower Jurassic Badaowan Formation. The relative percentage of Triassic zircon ages shows dramatic decrease from Xiaoquangou Group (Sample 17HJG-01) to Badaowan Formation (Sample Hao-01), probably revealing sources from Bogda Mountains have been eroded. We propose this is a slight uplift accompany by rapid denudation process during the Middle–Late Triassic.

5.2 Source-to-sink system of SJB in the Middle–Late Triassic

The detrital zircon U–Pb age probability and the Multidimensional scaling (MDS) plots were used in conjunction to establish the Middle–Late Triassic source-to-sink system of SJB (Figs. 5 and 10; Vermeesch, 2018). In the MDS plot, the thirteen samples from the Middle–Upper Triassic Xiaoquangou Group in SJB show distinct differences that generate four groups (Fig. 10).

Samples 15C-33, 16DLK-49 and 17HJG-01 (group 1) from the Well C, Xidalongkou and Haojiagou sections differ significantly from others due to high contents of Triassic zircons (Figs. 5 and 10), indicating a predominant contribution from the Bogda Mountains. Moreover, the samples from the Well C, Xidalongkou and Haojiagou sections contain subordinate the Carboniferous and Cambrian–Devonian zircons revealing that the NTS and CTS also provided sediments to the northern Bogda Mountains (Fig. 5). That is, the provenance of the Well C, Xidalongkou and Haojiagou sections are primarily attributed to the Bogda Mountains, with secondary contribution from the NTS and CTS.

Samples XJ12-06, 16TDG-06, and 17DDLK-09 (group 2) from the Aiweiergou, Taodonggou and Dongdalong sections are assigned similar sediment sources owing to their close links in the MDS plot (Fig. 10). The Mississippian and the Cambrian–Devonian magmatic rocks from the CTS are likely major sources for group 2, considering the relation of their spectra (Fig. 5). Group 2 also displays minor Pennsylvanian zircon grains in the detrital zircon U–Pb age probability plot that are likely related to the NTS sources.

Samples 12SKS-07, 17JGMK-06, and 16DBC-04 (group 3) from the Sikeshu, Jiangongmeikuang, and Dabancheng sections generally display a limited age variation dominated by the Pennsylvanian (Fig. 5), and show proximity in the MDS plot (Fig. 10). The Pennsylvanian age distribution combined with the compositionally and texturally immature detrital grains, probably originate from the magmatic rocks of NTS with zircon U–Pb ages of 320–300 Ma (Fig. 5). Furthermore, a little Cambrian–Devonian and Mississippian age groups in the probability plot also suggest contribution to group 3 from the CTS. Particularly, the probability plot of detrital zircon ages for the Dabancheng section (sample 16DBC-04) shows an age group spanning 250–200 Ma, reflecting further contribution from the Bogda Mountains to the Dabancheng section.

Samples 15HXG-95, 17JJZG-10, 17BYH-61, and HX-01 (group 4) from the Haxionggou, Jingjingzigou, Baiyanghe and Yuergou sections show a mixture age variation of Pennsylvanian (320–300 Ma) and Mississippian (360–320 Ma), and have proximity in the MDS plot (Fig. 10). The two major peaks with

age group spanning 320–300 Ma and 360–320 Ma, revealing the major provenance of group 4 is from NTS and CTS. Besides, the presence of some Triassic zircons in sample HX-01 from the Yuergou section suggests possible provenance from the Bogda Mountains.

The systematic analysis of the detrital zircons preserved in the Xiaoquangou Group allowed us to discriminate their source areas and establish the source-to-sink system in the Middle–Late Triassic for SJB. The provenance analysis of thirteen samples partitions SJB and adjacent areas into four groups (Fig. 11), which is consistent with groups from the MDS plot (Fig. 10). The Bogda Mountains, CTS, and NTS appear to be the dominant sources for group 1, group 2, and group 3, respectively (Fig. 10). The mixture of NTS and CTS appear to be the dominant sources for group 4 (Fig. 10). Although the source areas of SJB include the Bogda Mountains, NTS, and CTS in the Middle–Late Triassic, the western (NTS areas) and eastern (Bogda Mountains areas) parts of SJB exhibit inconsistencies in provenance patterns. In the Bogda Mountains, the provenance is attributed to the Bogda Mountains itself, NTS and CTS (Figs. 10 and 11). Of these, the Bogda sources mainly supply near regions, such as Haojiagou section, Xidalongkou section and Well C. In contrast, the NTS piedmont (the Sikeshu and Jiangongmeikuang sections) received detritus mainly from the NTS, with minor input from the CTS and no from the Bogda Mountains. In conclusion, the NTS accounts primarily for provenance of the western part of SJB (NTS areas), while sediments of the eastern part of SJB (Bogda Mountains areas) are principally from the Bogda Mountains and/or CTS (Figs. 3, 5, 10, 11).

5.3 Implication for the initial uplift of the Bogda Mountains

The Middle–Upper Triassic Xiaoquangou Group in the Well C, Haojiagou and Xidalongkou sections yields a complex age population with many syndepositional Triassic zircons from the Bogda Mountains (Fig. 5), indicating the initiation of sediment supply from the Bogda Mountains in the same area. We attribute this abrupt change to the initial uplift of the Bogda Mountains (referred as uplift stage; Wang et al. 2019b). Moreover, the Xiaoquangou Group in the Haojiagou and Xidalongkou sections contain lithic fragments (Wang et al. 2018b, 2019b), with the sediments characterized by moderate chemical weathering and sedimentary recycling (Wang et al. 2019a, 2019b). This suggests that the Bogda Mountains provided syndepositional magmatic rocks and recycled siliciclastics to the basin, probably pointing to a “sink–source–sink” process. In the cumulative frequency curves of the lag time (lag time = crystallization age – deposition age; Fig. 12), the sediments of the uplift stage show a near “bimodal lag time” including low and high lag time groups compared to mainly low lag time groups for the syn-rift and post-rift sediments (Fig. 12). The high lag time sediments probably arise from sedimentary recycling, while the low lag time sediments are attributed to the syndepositional magmatic activity. In addition, although the proportions of the Cambrian–Devonian, Mississippian, Pennsylvanian, and Permian populations diminish, these do not vanish compared to the underlying units (Wang et al. 2018b, 2019b). This implies that both the NTS and CTS continue providing sediments for sedimentation in the Bogda Mountains. This is further evidenced by the detrital-zircon U–Pb age cumulative frequency curves and the probability plot, which exhibit zircon age groups like the syn-rift and post-rift sediments (Figs. 5 and 12). We attribute this to Late

Triassic uplift of the Bogda Mountains, although the relatively smooth relief of its topography allowed scouring by rivers and consequently the supply of detritus from the NTS and CTS (Figs. 3 and 11).

6. Conclusions

Comparison of the detrital zircon U–Pb age distributions enabled constraining of the location of the Triassic magmatic activity in the SJB area. The comparison of the new detrital zircon U–Pb age dataset for the Middle–Upper Triassic Xiaoquangou Group of SJB shows that the Triassic magmatic activity occurred mainly in the Urumqi–Jimusaer area. The REEs abundance of the zircons reveal that the Triassic magmatism produced intermediate–acidic rocks. The geochronology data combined with provenance analysis indicates that provenance varies for different areas in SJB and adjacent areas, resulting in four sink areas. The Bogda Mountains started to supply sediments in the Late Triassic, marking the initial uplift of the Bogda Mountains. This study corroborates the utility of the comparison of detrital zircon U–Pb age distributions for identifying source locations. This suggests an effective approach for deciphering source characteristics when the potential source areas lack direct field evidence of related detrital-zircon U–Pb ages.

Declarations

Data availability

All data generated or analysed during this study are included in this published article (and its Supplementary Information files).

Acknowledgements

We appreciate the constructive comments from Prof. Zhaojie Guo, Prof. Baofu Han, Prof. Ping Guan, associate Prof. Qiugen Li, associate Prof. Lin Dong, and Dr. Yuanyuan Zhang. We are also grateful for the field assistance of Yuming Qi, Hongwei Li, Yizhe Wang and Jian Ma. We would like to thank Editage (www.editage.com) for English language editing. This study was supported by the National Science and Technology Major Project of China grant (2017ZX05008-001).

Author contributions

J.W. and C.W. wrote the main manuscript text, J.W. and Y.J. prepared Figures, and B.Y. conducted field investigations. All authors reviewed the manuscript.

Competing interests

The authors declare no competing interests.

References

1. Allen, M.B., Sengör, A.M.C. & Natal'in, B.A. Junggar, Turfan, and Alakol basins as Late Permian to ? Early Triassic extensional structures in a sinistral shear zone in the Altaid orogenic collage, Central Asia. *J. Geol. Soc,* **152,** 327-338 (1995).
2. Andersen, T. Correction of common lead in U–Pb analyses that do not report ^{204}Pb. *Chem. Geol.* **192,** 59-79 (2002).
3. Anderson, T. Detrital zircons as tracers of sedimentary provenance: limiting conditions from statistics and numerical simulation. *Chem. Geol.* **216,** 249-270 (2004).
4. Bhattacharya, J.P., Copeland, P., Lawton, T.F. & Holbrook, J. Estimation of source area, river paleo-discharge, paleoslope, and sediment budgets of linked deep-time depositional systems and implications for hydrocarbon potential. *Earth-Sci. Rev.* **153,** 77-110 (2016).
5. Belousova, E.A., Griffin, W.L., O'Reilly, S.Y. & Fisher, N.I. Igneous zircon: trace element composition as an indicator of source rock type. *Contrib. Mineral. Petr.* **143,** 602-622 (2002).
6. BGMRXUAR (Bureau of Geology and Mineral Resources of Xinjiang Uygur Antonomous Region). *Geological Publishing House,* 1–762 (1993).
7. Carroll, A.R., Graham, S.A. and Hendrix, M.S. Late Paleozoic tectonic amalgamation of northwestern China: sedimentary record of the northern Tarim, northwestern Turpan, and southern Junggar Basins. *Geol. Soc. Am. Bull.* **107,** 571–594 (1995).
8. Carroll, A.R., Graham, S.A. & Smith, M.E. Walled sedimentary basins of China in *Tectonic and stratigraphic evolution of nonmarine basins of China* (ed. Graham, S.A., Carroll, A.R. & Ping, L.). *Basin Res.* **22,** 17–32 (2010).
9. Cawood, P.A. & Nemchin, A.A. Provenance record of a rift basin: U/Pb ages of detrital zircons from the Perth basin, western Australia. *Sediment. Geol.* **134,** 209–234 (2000).
10. Cawood, P.A., Hawkesworth, C.J. & Dhuime, B. Detrital zircon record and tectonic setting. *Geology.* **40,** 875–878 (2012).
11. Corfu, F., Hanchar, J.M., Hoskin, P.W.O. & Kinny, P. Atlas of zircon textures. *Rev. Mineral. Geochem.* **53,** 469–500 (2003).
12. Fang, S.H. *et al.* New view on the Permian evolution of the Junggar Basin and its implications for tectonic evolution. *Earth Sci. Front.* **13,** 108–121 (2006).
13. Fang, Y.N *et al.* Provenance of the southern Junggar Basin in the Jurassic: Evidence from detrital zircon geochronology and depositional environments. *Sedimentary Geology.* **315,** 47–63 (2015).
14. Gao, J., Li, M.S., Xiao, X.C., Tang, Y.Q. & He, G.Q. Paleozoic tectonic volution of the Tianshan Orogen, northwestern China. *Tectonophysics.* **287,** 213–231(1998).
15. Gehrels, G. Detrital zircon U–Pb geochronology applied to tectonics. *Annu. Rev. Earth Pl. Sci.* **42,** 127–149 (2014).
16. Greene, T.J. *et al.* Sedimentary record of Mesozoic deformation and inception of the Turpan–Hami basin, northwest China. in Paleozoic and Mesozoic tectonic evolution of central Asia: From

continental assembly to intracontinental deformation (ed. Hendrix, M.S. & Davis, G.A.). *Boulder, Colorado, Geological Society of America Memoir.* **194,** 317–340 (2001).

17. Greene, T.J., Carroll, A.R., Wartes, M.A., Graham, S.A. & Wooden, J.L. Integrated provenance analysis of a complex orogenic terrane: Mesozoic uplift of the Bogda Shan and inception of the Turpan–Hami basin, NW China. *J. Sediment. Res.* **75,** 251–267 (2005).
18. Gu, L.X.*et al.* Carboniferous volcanites in the Bogda orogenic belt of eastern Tianshan: their tectonic implications. *Acta Petrol. Sin.* **16,** 305–316 (2000).
19. Gu, L.X. *et al.* Intrusive activities during compression–extension tectonic conversion in the Bogda intracontinental orogen. *Acta Petrol. Sin.* **17,** 187–198 (2001).
20. Hampson, G.J., Duller, R.A., Petter, A.L., Robinson, R.A.J. & Allen, P.A. Mass–balance constraints on stratigraphic interpretation of linked Alluvial–Coastal–Shelfal Deposits from Source to Sink: Example from Cretaceous Western Interior Basin, Utah and Colorado, U.S.A. *J. Sediment. Res.* **84,** 935–960 (2014).
21. Han, B.F. *et al.* Age, geochemistry, and tectonic implications of a late Paleozoic stitching pluton in the North Tian Shan suture zone, western China. *Geol. Soc. Am. Bull.* **122,** 627–640 (2010).
22. Han, B.F., He, G.Q., Wang, X.C. & Guo, Z.J. Late Carboniferous collision between the Tarim and Kazakhstan–Yili terranes in the western segment of the South Tian Shan Orogen, Central Asia, and implications for the Northern Xinjiang, western China. *Earth-Sci. Rev.* **109,** 74–93 (2011).
23. an, Y. & Zhao, G. Final amalgamation of the Tianshan and Junggar orogenic collage in the southwestern Central Asian Orogenic Belt: constraints on the closure of the Paleo-Asian Ocean. *Earth-Sci. Rev.* **186,** 129–152 (2018).
24. Hoskin, P.W.O. and Ireland, T.R. Rare earth element chemistry of zircon and its use as a provenance indicator. *Geology.* **7,** 627–630 (2000).
25. Jackson, S.E., Pearson, N.J., Griffin, W.L. & Belousova, E.A. The application of laser ablation-inductively coupled plasma-mass spectrometry to in situ U–Pb zircon geochronology. *Chem. Geol.* **211,** 47–69 (2004).
26. Ji, H. *et al.* Early to Middle Jurassic tectonic evolution of the Bogda mountains, northwest China: evidence from sedimentology and detrital zircon geochronology. *J. Asian Earth Sci.* **153,** 57–74 (2018).
27. Li, D., He, D., and Tang, Y. Reconstructing multiple arc-basin systems in the Altai–Junggar area (NW China): Implications for the architecture and evolution of the western Central Asian Orogenic Belt. *J. Asian Earth Sci.* **12,** 84–107 (2016).
28. Li, Z., Tang, W. X., Peng, S. T. & Xu, J. Q. Detrital zircon U-Pb geochronological and depositional records of the Mesozoic–Cenozoic profile in the southern Junggar Basin, NW China, and their responses to basin-range tectonic evolution. *Chin. J. Geol.* **47,** 1016–1040 (2012).
29. Liu, D.D., Guo, Z.J. & Zhang, Z.Y. A new viewpoint of the Aiweiergou Unconformity, northern Tian Shan, Xinjiang. *Geotectonica et Metallogenia.* **37,** 349–365 (2013).

30. Liu, D.D. *et al.* What generated the Late Permian to Triassic unconformities in the southern Junggar Basin and western Turpan Basin; tectonic uplift, or increasing aridity? Palaeogeogr. *Palaeoclimatol. Palaeoecol.* **468,** 1–17 (2017).
31. Liu, D.D. *et al.* Provenance and geochemistry of lower to Middle Permian strata in the southern Junggar and Turpan Basins: a terrestrial record from mid-latitude NE Pangea. *Palaeogeogr. Palaeoclimatol. Palaeoecol.* **495,** 259–277 (2018).
32. Ludwig, K.R. ISOPLOT 3: A geochronological toolkit for Microsoft Excel. Berkeley. *Berkeley Geochronology Centre Special Publication.* 1–74 (2003).
33. Michael, N.A., Whittaker, A.C., Carter, A. & Allen, P.A. Volumetric budget and grain–size fractionation of a geological sediment routing system: Eocene Escanilla Formation, south–central Pyrenees. *Geol. Soc. Am. Bull.* **126,** 585–599 (2014).
34. Nie, J.S. *et al.* Integrated provenance analysis of a convergent retroarc foreland system: U–Pb ages, heavy minerals, Nd isotopes, and sandstone compositions of the Middle Magdalena Valley basin, northern Andes, Colombia. *Earth-Sci. Rev.* **110,** 111–126 (2012).
35. Nguyen, H.H., Carter, A., Hoang, L.V. & Vu, S.T. Provenance, routing and weathering history of heavy minerals from coastal placer deposits of southern Vietnam. *Sediment. Geol.* **373,** 228–238 (2018).
36. Obrist-Farner, J. & Yang, W. Nonmarine time-stratigraphy in a rift setting —An example from the mid-Permian lower Quanzijie low-order cycle, Bogda Mountains, NW China. *J. Palaeog.-English.* **4,** 27–51 (2015).
37. Obrist-Farner, J. & Yang, W. Provenance and depositional conditions of fluvial conglomerates and sandstones and their controlling processes in a rift setting, mid-Permian lower and upper Quanzijie low order cycles, Bogda Mountains, NW China. *J. Asian Earth Sci.* **138,** 317–340 (2017).
38. Olierook, H.K.H. *et al.* Tectonic controls on sediment provenance evolution in rift basins: Detrital zircon U–Pb and Hf isotope analysis from the Perth Basin, Western Australia. *Gondwana Res.* **66,** 129–142 (2019).
39. Romans, B.W., Castelltort, S., Covault, J.A., Fildani, A. & Walsh, J.P. Environmental signal propagation in sedimentary systems across timescales. *Earth-Sci. Rev.* **153,** 7–29 (2016).
40. Şengör, A.M.C., Natal'in, B.A. & Burtman, U.S. Evolution of the Altaid tectonic collage and Palaeozoic crustal growth in Eurasia. *Nature.* **364,** 299–307 (1993).
41. Sømme, T.O., Jackson, A.L. & Vaksdal, M. Source–to–sink analysis of ancient sedimentary systems using a subsurface case study from the Møre–Trøndelag area of southern Norway: part 1 – depositional setting and fan evolution. *Basin Res.* **25,** 489–511 (2013).
42. Sømme, T.O. & Jackson, A.L. Source–to–sink analysis of ancient sedimentary systems using a subsurface case study from the Møre–Trøndelag area of southern Norway: part 2 – sediment dispersal and forcing mechanisms. *Basin Res.* **25,** 512–531 (2013).
43. Sun, S.S. & McDonough, W.F. Chemical and isotopic systematics of oceanic basalts: implications for mantle composition and processes. In Saunders, A.D.; and Norry, M.J. Eds. Magmatism in the Ocean Basins. *Geol.Soc. London, Special Publication.* **423,** 313–345 (1989).

44. Tang, W.H. *et al.* Late Paleozoic to Jurassic tectonic evolution of the Bogda area (northwest China): Evidence from detrital zircon U–Pb geochronology. *Tectonophysics.* **626,** 144–156 (2014).
45. Thompson, J. Meffre, S. & Danyushevsky, L. Impact of air, laser pulse width and fluence on U-Pb dating of zircons by LA-ICPMS. *Journal of Analytical Atomic Spectrometry* **33,** 221–230 (2018).
46. Vermeesch, P. IsoplotR: a free and open toolbox for geochronology. *Geosci. Front.* **9,** 1479–1493 (2018).
47. Wang, J.L. & Li, Z. Trace element compositions in the detrital zircons as an indicator of source rock type: An example from the Liaohe Group in the Liaodong Peninsula, northeast China. *Geol. Sci. Technol. Inform.* **3,** 36–50 (2017).
48. Wang, J.L. *et al.* Tectonic–depositional environment and prototype basin evolution of the Permian–Triassic in the southern Junggar Basin. *J. Palaeogeog.* **18,** 643–660 (2016).
49. Wang, J.L. *et al.* Geochronology and geochemistry of volcanic rocks in the Arbasay Formation, Xinjiang Province (Northwest China): implications for the tectonic evolution of the North Tianshan. *Int. Geol. Rev.* **59,** 1324–1343 (2017).
50. Wang, J.L. *et al.* Age assignment of the upper Carboniferous Arbasay Formation in the Shichang Region, North Tianshan (NW China). *J. Palaeogeog.-English.* **7,** 272–282 (2018a).
51. Wang, J.L. *et al.* The tectonic evolution of the Bogda Mountains from Late Carboniferous to Triassic time: evidence from detrital zircon U–Pb geochronology and sandstone petrography. *Geol. Mag.* **155,** 1063–1088 (2018b).
52. Wang, J.L. *et al.* Whole-rock geochemistry and zircon Hf isotope of Late Carboniferous–Triassic sediments in the Bogda region, NW China: Clues for provenance and tectonic setting. *Geol. J.* **54,** 1853-1877 (2019a).
53. Wang, J.L. *et al.* Source-to-sink analysis of a transtensional rift basin from syn-rift to uplift stages. *J. Sediment. Res.* **89,** 335–352 (2019b).
54. Wartes, M.A., Carroll, A.R. & Greene, T.J. Permian sedimentary record of the Turpan–Hami basin and adjacent regions, northwest China: Constraints on postamalgamation tectonic evolution. *Geol. Soc. Am. Bull.* **114,** 131–152 (2002).
55. Windley, B.F., Alexeiev, D., Xiao, W., Kröner, A. & Badarch, G. Tectonic models for accretion of the Central Orogenic Belt. *J. Geol. Soc. London.* **164,** 31–47 (2007).
56. Wu, L. et al. Multiple provenance of rift sediments in the composite basin–mountain system: Constraints from detrital zircon U–Pb geochronology and heavy minerals of the early Eocene Jianghan Basin, central China. *Sediment. Geol.* **349,** 46–61 (2017).
57. Xiao, W.J. *et al.* Middle Cambrian to Permian subduction-related accretionary orogenesis of Northern Xinjiang, NW China: Implications for the tectonic evolution of central Asia. *J. Asian Earth Sci.* **32,** 102–117 (2008).
58. Xiao, W.J, Windley, B.F., Allen, M.B. & Han, C.M. Paleozoic multiple accretionary and collisional tectonics of the Chinese Tianshan orogenic collage. *Gondwana Res.* **23,** 1316–1341 (2013).

59. Yang, D.B. *et al.* U–Pb ages and Hf isotope data from detrital zircons in the Neoproterozoic sandstones of northern Jiangsu and southern Liaoning Provinces, China: Implications for the Late Precambrian evolution of the southeastern North China Craton. *Precambrian Res.* **216,** 162– 176 (2012).
60. Yang, W. *et al.* Sedimentary evidence of Early–Late Permian mid-latitude continental climate variability, southern Bogda Mountains, NW China. *Palaeogeogr. Palaeoclimatol. Palaeoecol.* **252,** 239–258 (2007).
61. Yang, W. *et al.* Depositional environments and cyclo- and chronostratigraphy of uppermost Carboniferous–Lower Triassic fluvial–lacustrine deposits, southern Bogda Mountains, NW China ––A terrestrial paleoclimatic record of mid-latitude NE Pangea. *Global Planet. Change.* **73,** 15–113 (2010).
62. Yin, J.Y. *et al.* The thermal evolution of Chinese Central Tianshan and its implications: Insights from multi-method chronometry. *Tectonophysics.* **722,** 536–548 (2018).
63. Yuan, H.L. et al. Accurate U–Pb age and trace element determinations of zircon by laser ablation inductively coupled plasma mass spectrometry. *Geostand. Newsl.* **28,** 353–370 (2004).
64. Zhu, W. et al. Triassic provenance and its tectonic significance in Sikeshu Sag, Junggar Basin. *Xinjiang Petrol. Geol.* **38,** 512–518 (2017).

Figures

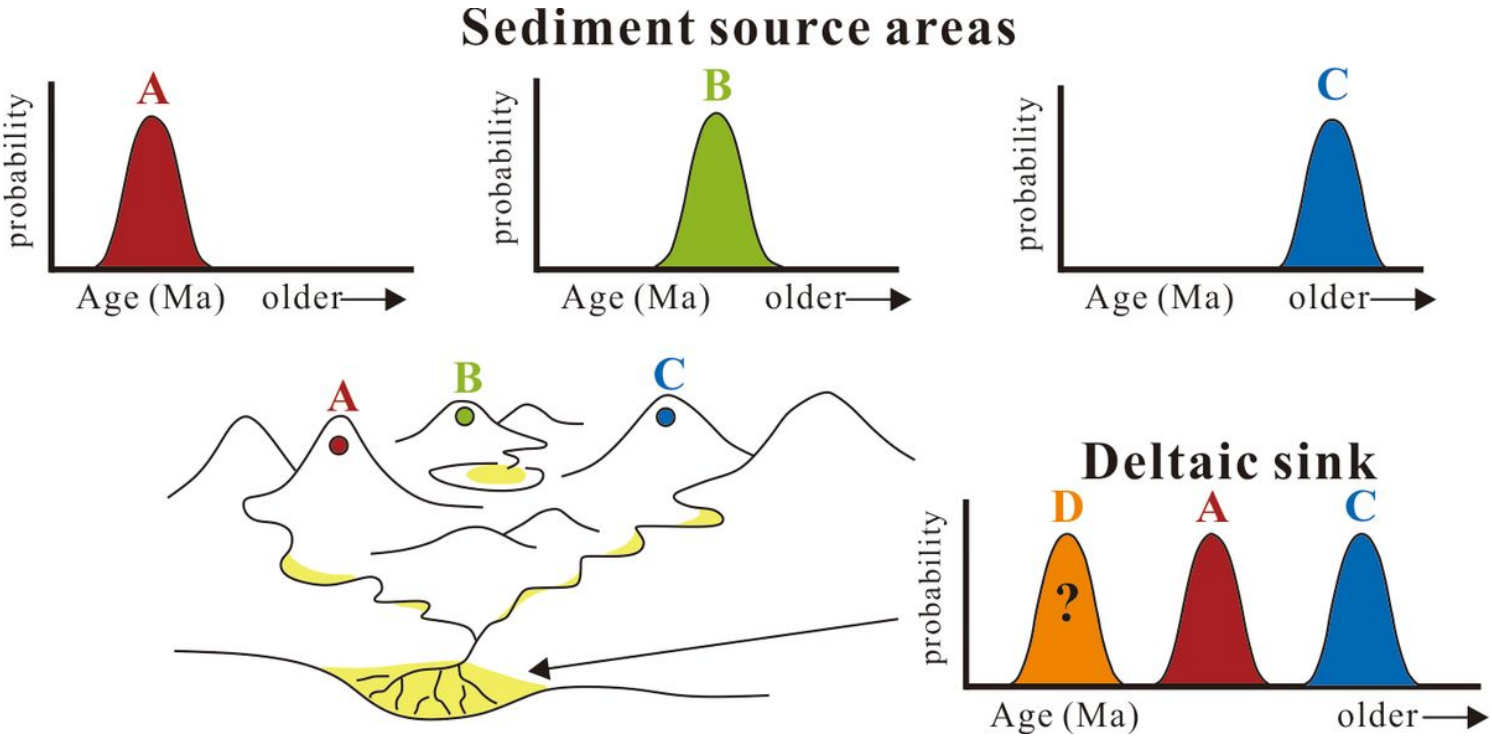

Figure 1

Conceptual diagram of deep-time source-to-sink analysis using detrital minerals, especially detrital zircon U–Pb geochronology (modified after Romans et al. 2016).

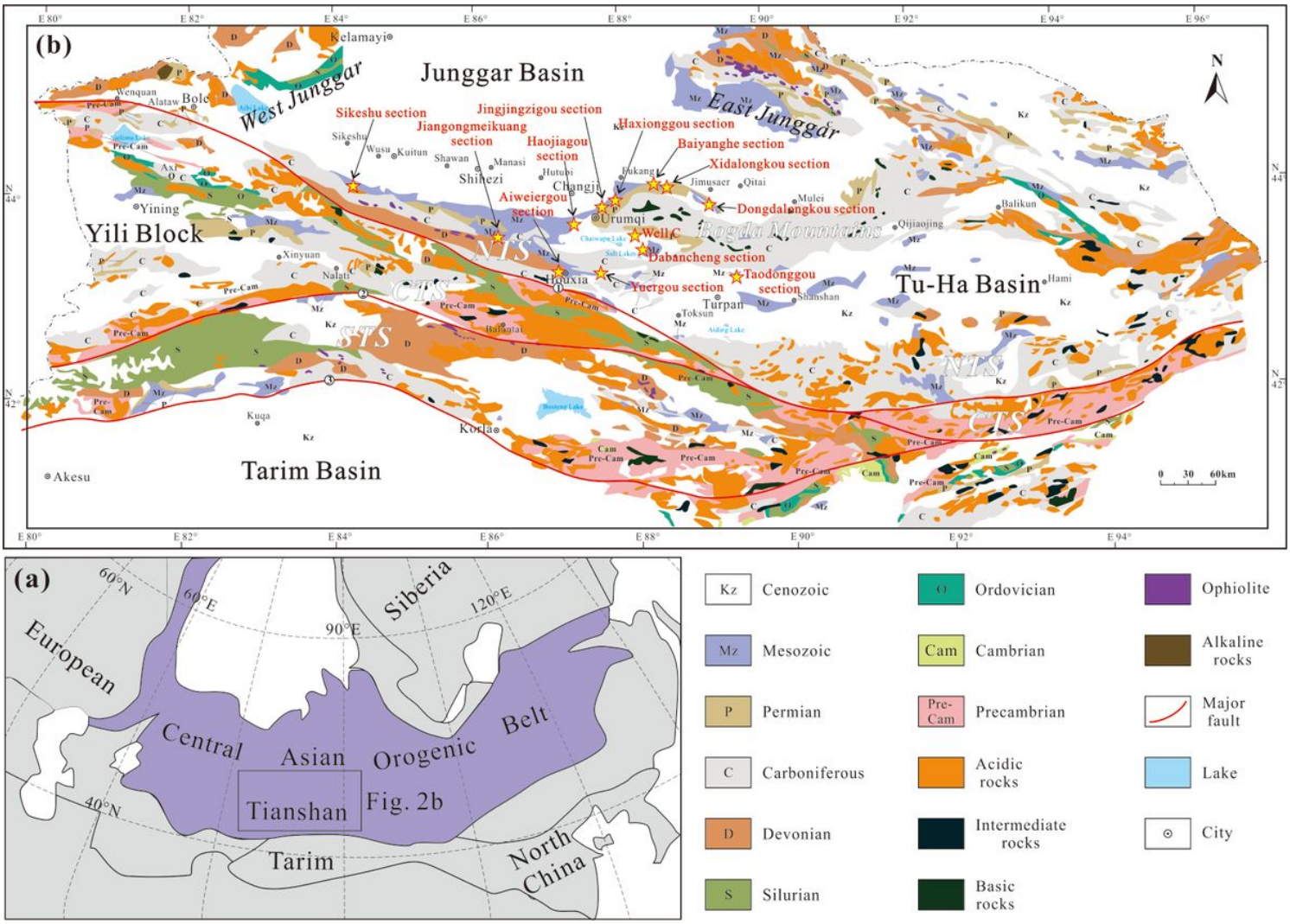

Figure 2

(a) Tectonic outlines of the Central Asian Orogenic Belt (modified after Han et al. 2010). (b) Tectonic map of the Tianshan and Southern Junggar Basin showing the location of the studied sections (star areas; modified after BGMRXUAR 1993; Wang et al. 2017). Note: The designations employed and the presentation of the material on this map do not imply the expression of any opinion whatsoever on the part of Research Square concerning the legal status of any country, territory, city or area or of its authorities, or concerning the delimitation of its frontiers or boundaries. This map has been provided by the authors.

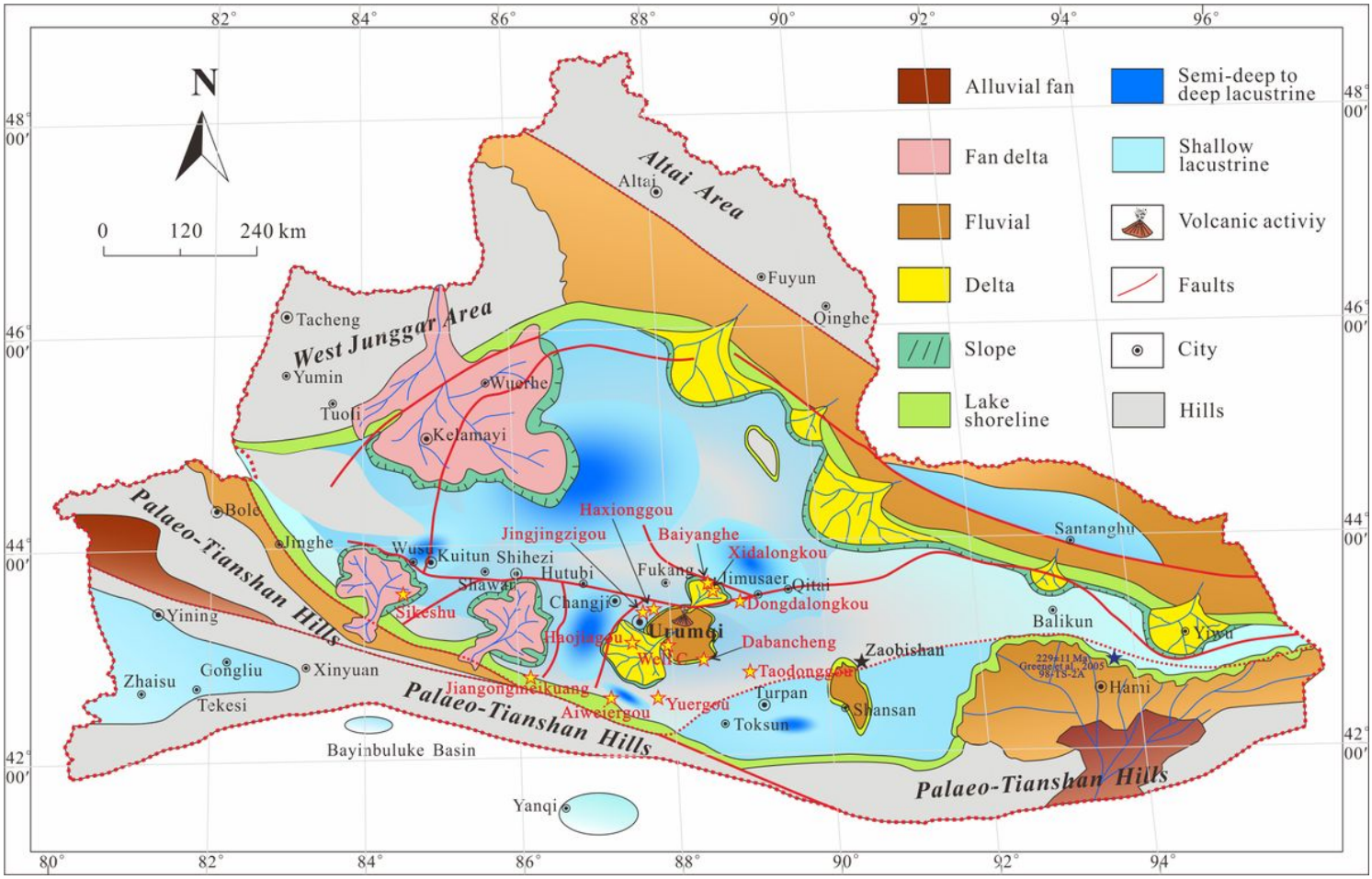

Figure 3

Paleogeographic map of the Junggar Basin and adjacent areas during the Middle–Late Triassic period. Note: The designations employed and the presentation of the material on this map do not imply the expression of any opinion whatsoever on the part of Research Square concerning the legal status of any country, territory, city or area or of its authorities, or concerning the delimitation of its frontiers or boundaries. This map has been provided by the authors.

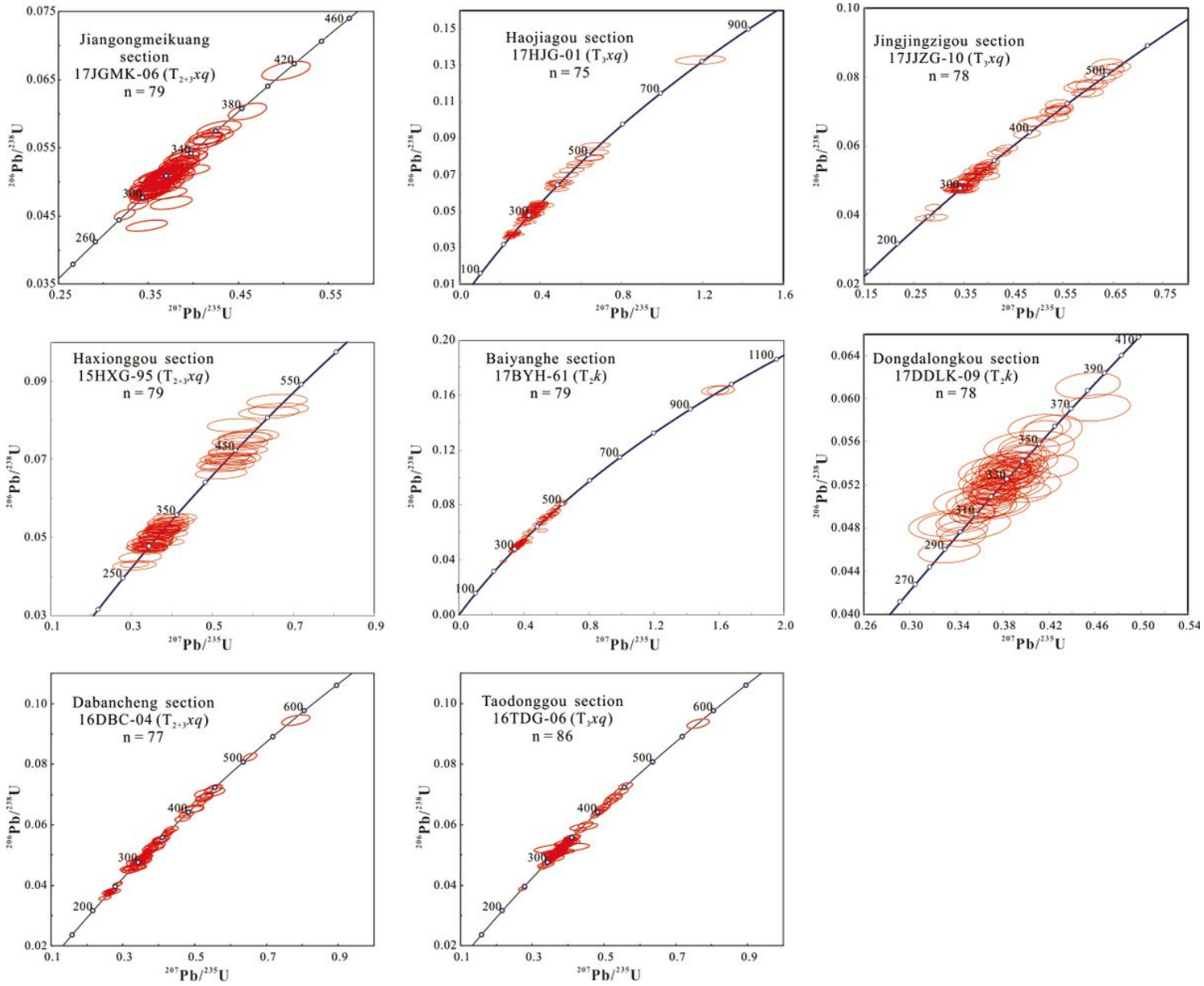

Figure 4

The U–Pb Concordia diagrams for zircons acquired from the Middle–Upper Triassic Xiaoquangou Group in different sections of the Southern Junggar Basin.

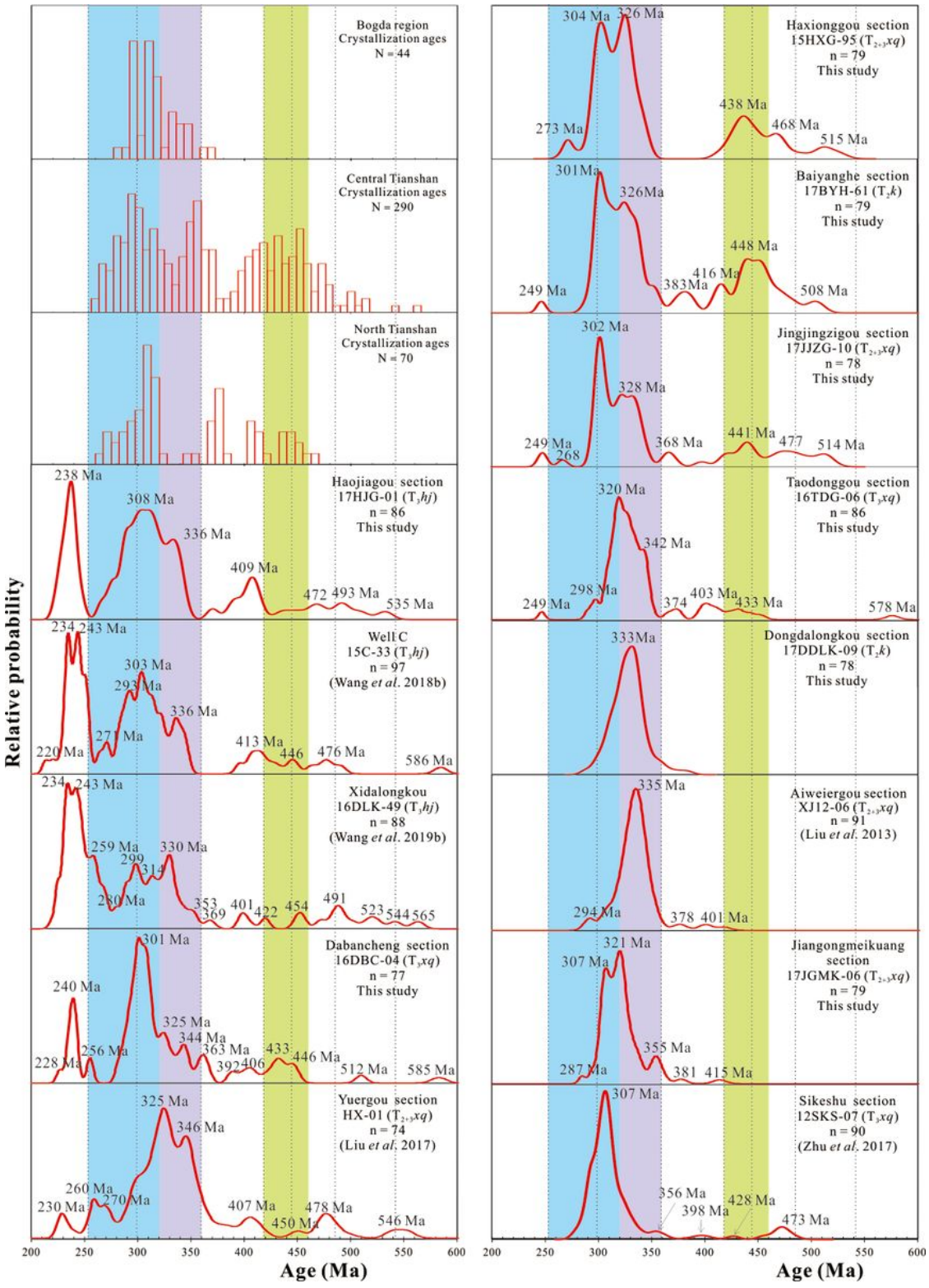

Figure 5

Relative U–Pb age probability plots of detrital zircons derived from the Middle–Upper Triassic Xiaoquangou Group in different sections of the Southern Junggar Basin. Histograms of crystallization ages from STS–Tarim, the Bogda Mountains, CTS, and NTS areas are also shown for comparison (see Wang et al. 2019b for data compilation).

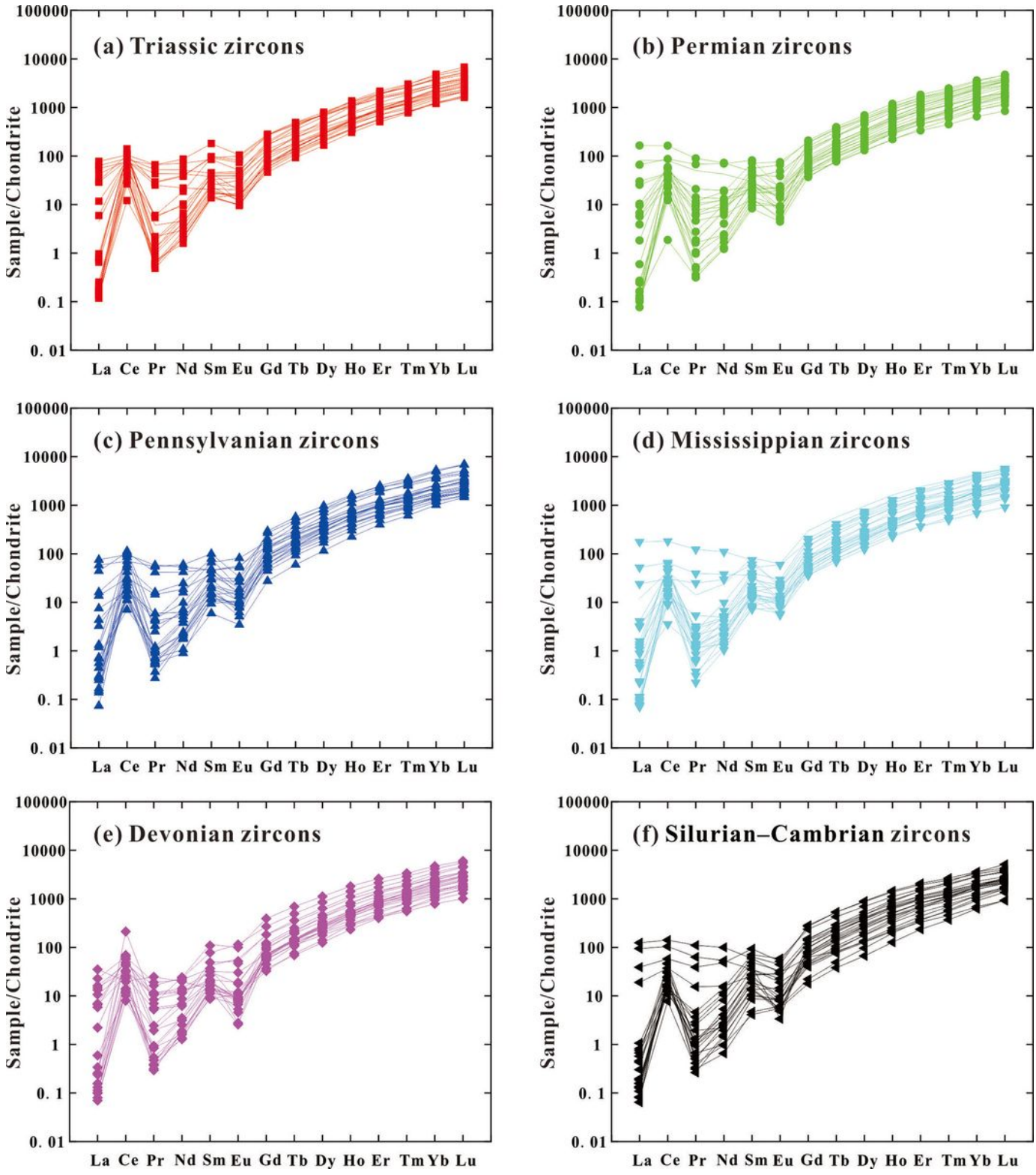

Figure 6

Chondrite–normalized REE patterns for the (a) Triassic, (b) Permian, (c) Pennsylvanian, (d) Mississippian, (e) Devonian, and (f) Silurian–Cambrian zircons. chondrite values are from Sun and McDonough (1989).

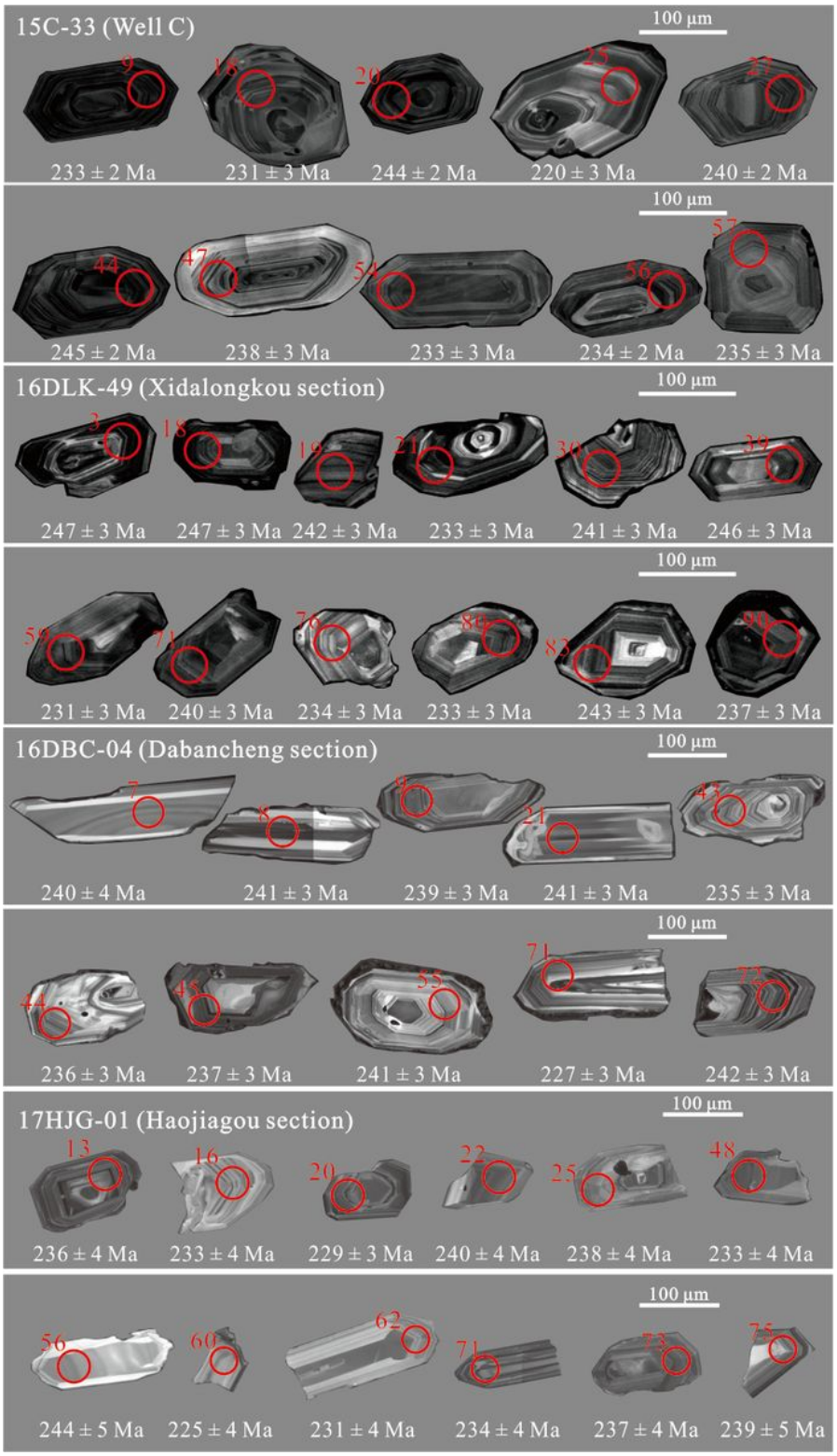

Figure 7

Representative cathodoluminescence (CL) images of the Triassic zircons.

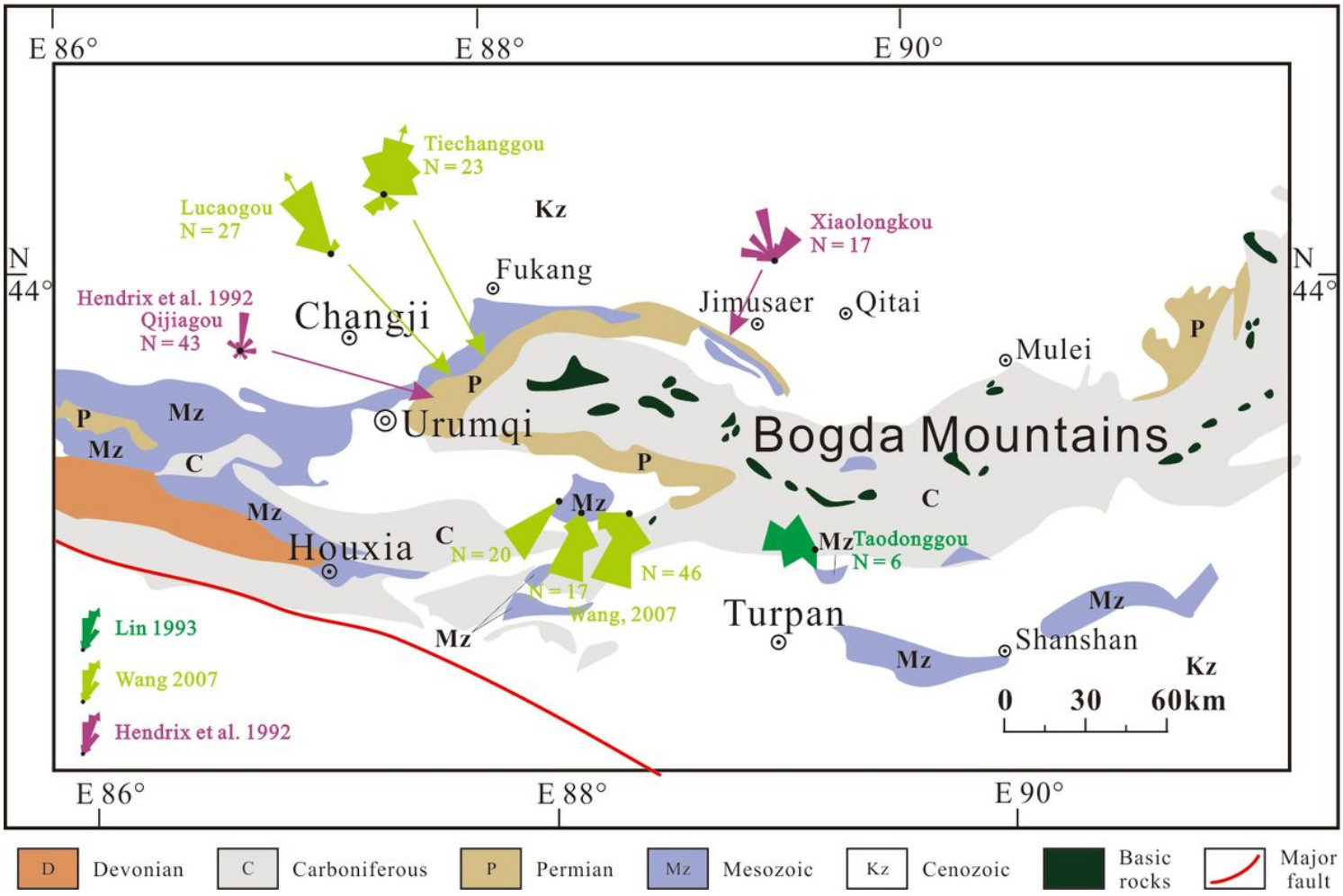

Figure 8

Paleocurrent directions of the Middle–Upper Triassic strata around the Bogda Mountains (Wang et al., 2019b). Note: The designations employed and the presentation of the material on this map do not imply the expression of any opinion whatsoever on the part of Research Square concerning the legal status of any country, territory, city or area or of its authorities, or concerning the delimitation of its frontiers or boundaries. This map has been provided by the authors.

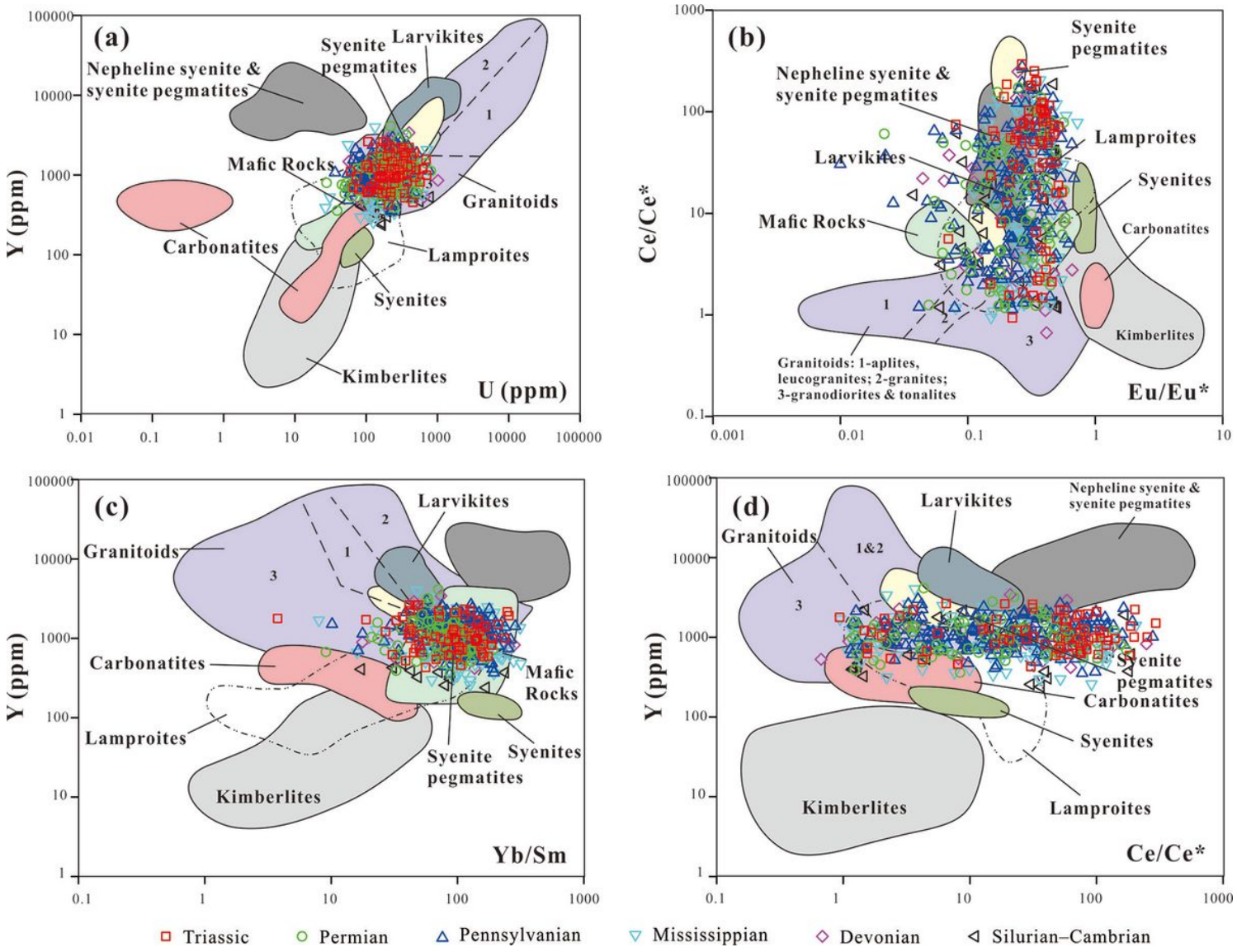

Figure 9

Zircon compositions of (a) U–Y, (b) Eu/Eu*–Ce/Ce*, (c) Yb/Sm–Y, and (d) Ce/Ce*–Y diagrams used as discriminants for different source rock types (modified after Belousova et al. 2002).

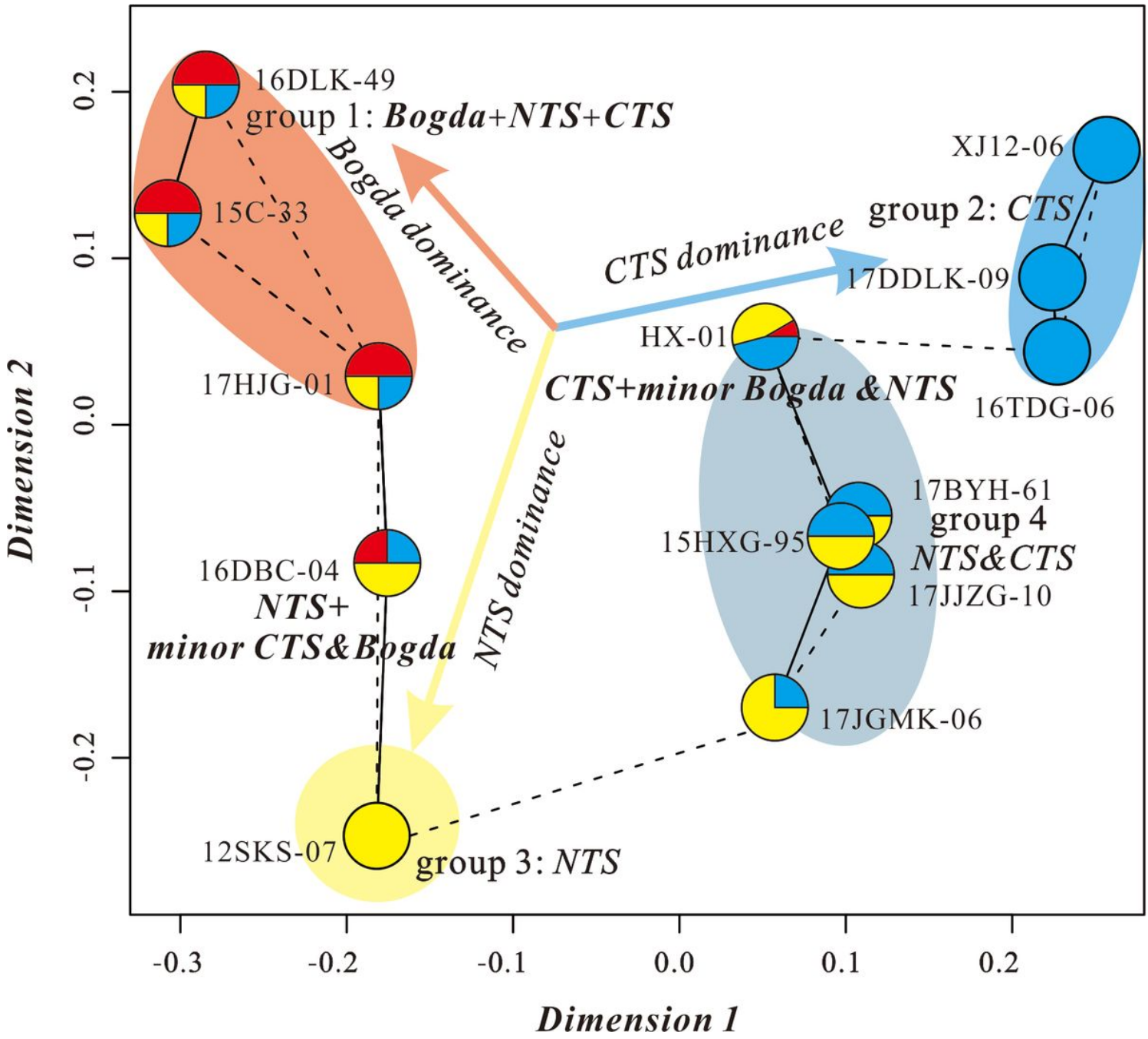

Figure 10

Multidimensional Scaling plots (MDS) for detrital zircon U–Pb data of the samples from the Middle–Upper Triassic Xiaoquangou Group in different measured sections of the Southern Junggar Basin (Vermeesch, 2018). Solid and dashed lines represent the closest and second closes neighbors, respectively. NTS, North Tianshan; CTS, Central Tianshan; Bogda, Bogda Mountains.

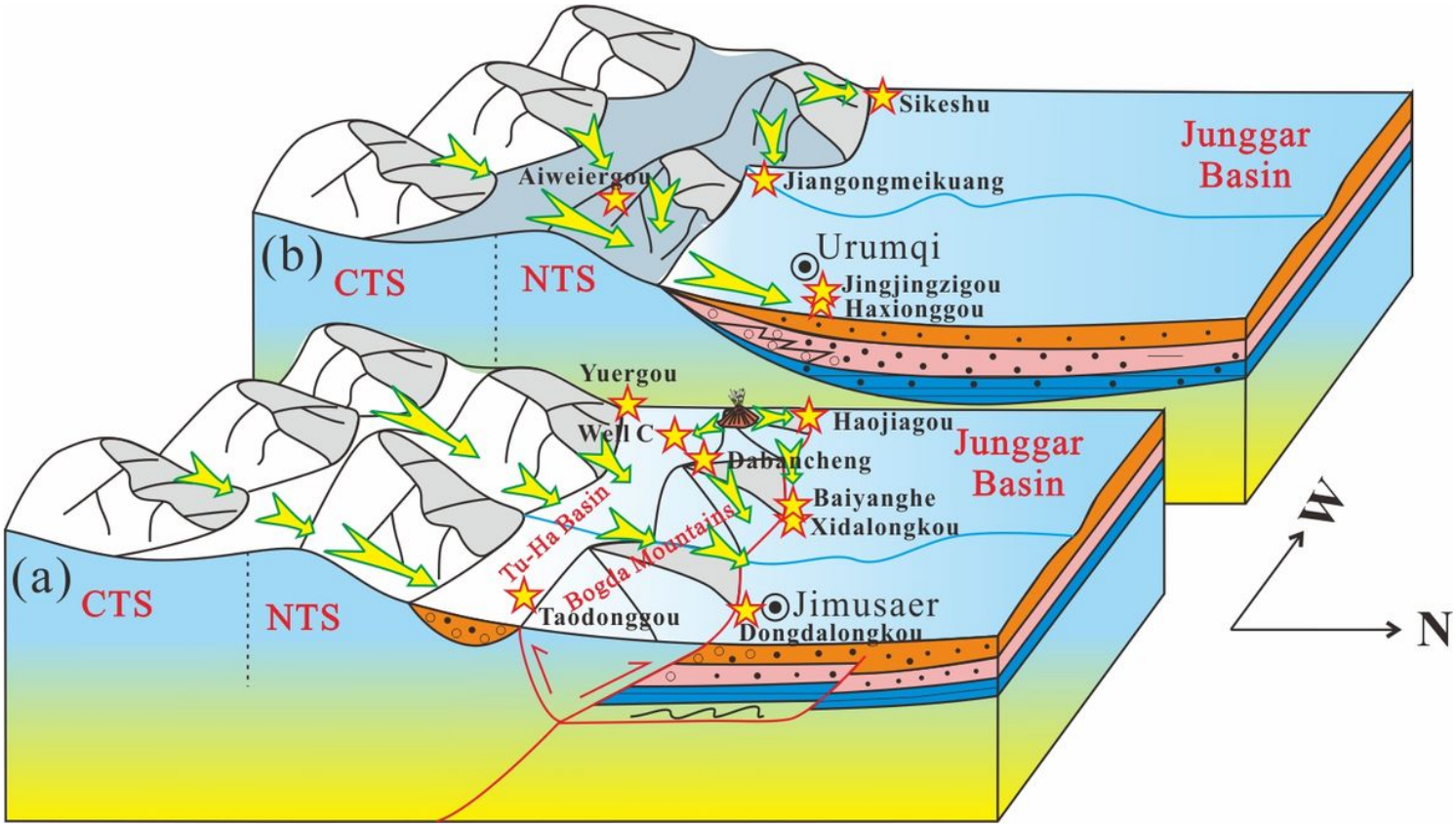

Figure 11

Schematic 3D diagram demonstrating the source-to-sink system of the Southern Junggar Basin and its adjacent areas in the Middle–Late Triassic. NTS, North Tianshan; CTS, Central Tianshan.

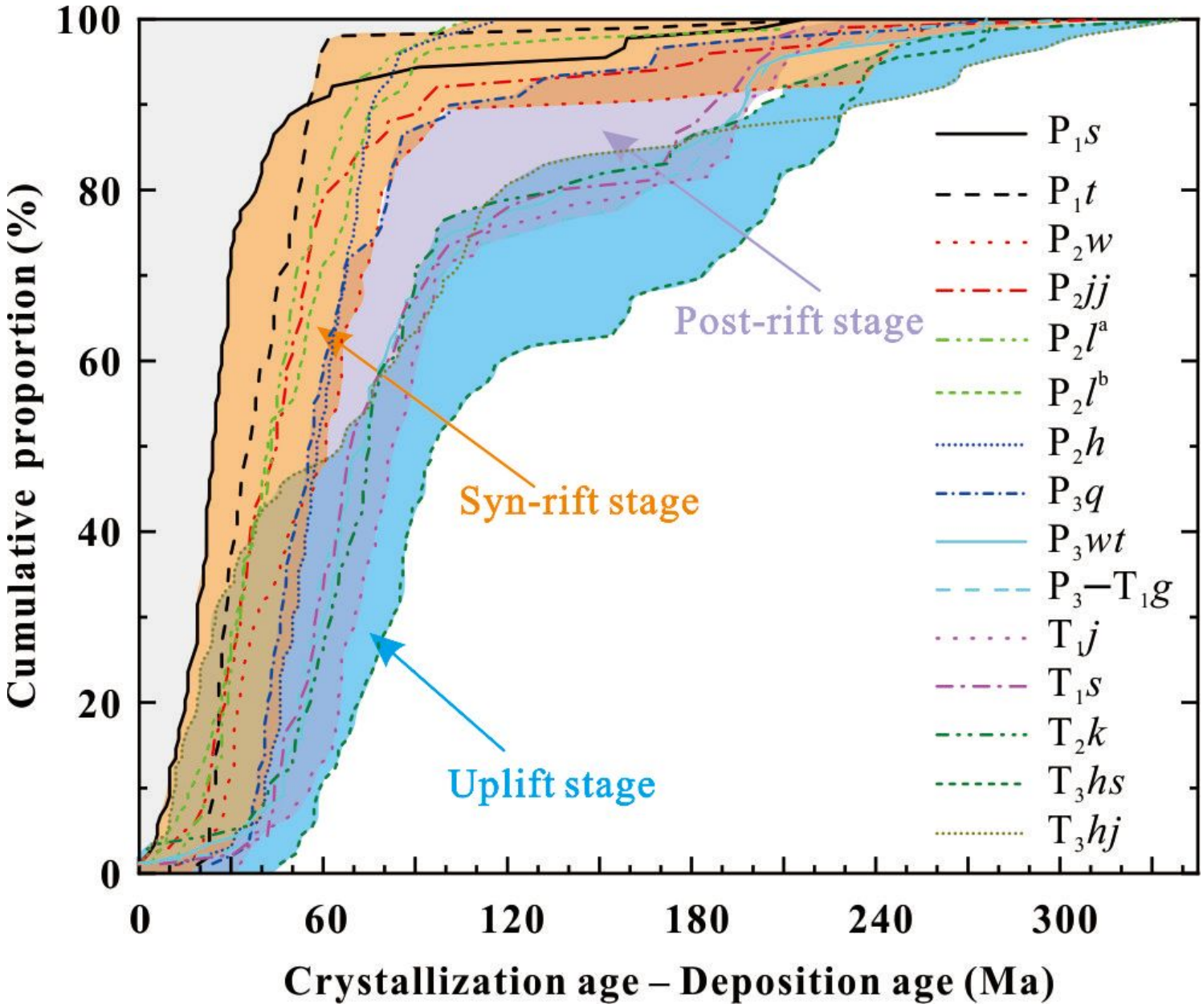

Figure 12

Cumulative frequency curves of the lag time (crystallization age – depositional age) for the Cisuralian Shirenzigou Formation to the Upper Triassic Haojiagou Formation. The data and tectonic evolution stages are from Wang et al. (2018b, 2019b). P1s, Shirenzigou Formation; P1t, Tashikula Formation; P2w, Wulapo Formation; P2jj, Jingjingzigou Formation; P2la, lower Lucaogou Formation; P2lb, upper Lucaogou Formation; P2h, Hongyanchi Formation; P3q, Quanzijie Formation; P3wt, Wutonggou Formation; P3–T1g, Guodikeng Formation; T1j, Jiucaiyuanzi Formation; T1s, Shaofanggou Formation; T2k, Kelamayi Formation; T3hs, Huangshanjie Formation; T3hj, Haojiagou Formation.

Supplementary Files

This is a list of supplementary files associated with this preprint. Click to download.

- SupplementalTables.xlsx